

# Snow depth estimation accuracy using a dual-interface GPS-IR model with experimental results

Qiang Chen<sup>1</sup> · Daehee Won<sup>1</sup> · Dennis M. Akos<sup>1</sup>

Received: 10 July 2015 / Accepted: 13 January 2016 / Published online: 27 January 2016  
© Springer-Verlag Berlin Heidelberg 2016

**Abstract** Measuring snow depth using the GPS interferometric reflectometry is an active microwave remote sensing technique and an emerging approach because of its relatively large spatial coverage and high temporal sampling capability. The current geodetic GPS networks are capable of measuring snow depth in the vicinity of the antenna installation at no additional hardware cost. However, the performance is constrained by the geodetic GPS antenna which was originally designed to minimize the reception of the reflected signal. In our prior work, we proposed a horizontally polarized antenna which has equal gain for both direct and reflected signals and tested its performance for a single snow event. In order to comprehensively assess its performance, we set up a horizontally polarized snow monitor (HPSM) using the improved antenna at Marshall, Colorado, USA, over the 2013–2014 water year. The data from the HPSM clearly shows that the proposed design has high sensitivity to even very light snowfalls. However, some anomalies are observed from the HPSM measurements, which tend to either overestimate or underestimate the actual snow depth. We explain the observed measurement anomalies by replacing the traditional air–snow single-interface model with an air–snow–soil dual-interface model. The effectiveness of the new model is validated by comparing the simulated results to

the HPSM measurements. Utilizing the dual-interface model, we simulate the error curve for snow depth estimation given various snow depths and snow permittivities. The error curve shows that the estimation biases can be observed only for shallow snow with a relatively small permittivity value.

**Keywords** GPS-IR · Snow depth · Horizontal polarization

## Introduction

Snowpack is an important component in the investigation of global climate and hydrology and fresh water reservoirs. The measurement of the amount of water stored in the snowpack and its melt rate are essential for the management of the water supply and flood control systems, and about one-sixth of the world population depends on snowpack for their fresh water supply (Armstrong and Brun 2008; Barnett et al. 2005; Shi and Dozier 2000). Among the various snow measuring techniques, the GPS interferometric reflectometry (GPS-IR) is an emerging approach with the advantages of relatively large spatial coverage compared to point-scale sensors (e.g., sonic) and high temporal sampling rate compared to airborne or space-based sensors (Gutmann et al. 2012; Larson et al. 2009). Larson et al. (2009) demonstrated that the current network of geodetic GPS stations which were installed for geophysical and surveying applications are capable of measuring snow depth in their vicinity by utilizing the signal-to-noise ratio (SNR) data of GPS satellites. The observed SNR shows peaks and troughs when the direct and the ground reflected signals go in and out of phase. A complete forward model of the SNR data from a geodetic

---

✉ Qiang Chen  
qiang.chen@colorado.edu

Daehee Won  
daehee.won@colorado.edu

Dennis M. Akos  
dma@colorado.edu

<sup>1</sup> Department of Aerospace Engineering Sciences, University of Colorado, Boulder, CO 80309, USA

GPS receiver (Nievinski and Larson 2014a; Zavorotny et al. 2010) and the inverse model for snow depth retrievals (Nievinski and Larson 2014b, c) were demonstrated in detail previously. The snow depth measurements from the GPS-IR at several geodetic GPS stations are compared with those measurements from SNOTEL, LIDAR, ultrasonic sensor, and manual measurement to show its viability and superiority.

The advantages of utilizing geodetic GPS data include the wide area coverage of the existing geodetic GPS networks as well as no additional hardware cost for this remote sensing capability expansion. However, the geodetic GPS antenna is not optimal for GPS-IR remote sensing: It is right-handed circularly polarized (RHCP), and its RHCP gain is optimized for the zenith direction to suppress reflected GPS signals (Zavorotny et al. 2010). In order to overcome the limitations of the geodetic antenna, we proposed a horizontally polarized dipole antenna (Chen et al. 2014) and have evaluated its performance in an experiment campaign conducted at Table Mountain, Boulder, Colorado, USA, during February 2012. The observed SNR data clearly show a more distinct interference pattern which yields more precise snow depth estimation with a tighter 95 % confidence interval.

In order to fully evaluate the performance of the proposed dipole antenna, we set up a horizontally polarized snow monitor (HPSM) at the University Corporation for Atmospheric Research (UCAR) experiment field in Marshall, Colorado, and carried out an experiment from November 2013 to May 2014. We set up a camera and a measurement post to monitor the snow depth in the sensing area. There exists a geodetic GPS station which belongs to the EarthScope Plate Boundary Observatory (PBO), and three SR50 ultrasonic snow sensors located near the HPSM. All the snow measurements from the three sensors (camera, PBO station, and SR50) are used to verify the snow depth measurement of the HPSM.

The HPSM detects each of the eleven snowfall events and gives the snow depth measurements, while the PBO receiver only provides measurements for a small portion of the snowfall events. However, the HPSM measurements show clear estimation biases for some of the snowfalls, by either underestimating or overestimating the snow depth compared to the ground truth data. These measurement anomalies cannot be simply explained as a result of noise since all GPS satellite data in the sensing area show a uniform trend. In order to explain the measurement anomalies, we develop a dual-interface model (air–snow–soil) to account for the effect of the soil medium under the snow layer as opposed to the air–snow single-interface model. The observed measurement anomalies are explained by the simulation results and validated against the ground truth data. Using the dual-interface model, we

simulate the estimation error curve by varying snow depths and permittivities. From the error curve, we conclude that the estimation biases can only be observed with shallow snow and the biases decrease to negligible when the snow depth increases.

## GPS-IR forward model and polarization selection

As stated earlier, GPS-IR utilizes the interference pattern of the observed SNR to infer the parameters of the earth environment. Here we review the GPS-IR model, present the characteristics of different polarizations, and demonstrate the horizontal polarization is optimal for snow sensing.

SNR is defined as the ratio of the signal power  $P_s$  to the noise power  $P_n$  and serves as an indicator of the signal strength. In a GPS receiver, carrier-to-noise ratio ( $C/N_0$ ), defined as the ratio of the signal power  $P_s$  to the noise power spectral density  $N_0$ , is more often used to exclude the effect of noise bandwidth that is receiver dependent. The relationship between SNR and  $C/N_0$  can be described by:

$$\text{SNR} = \frac{C/N_0}{B_n} \quad (1)$$

where  $B_n$  is the noise bandwidth in the GPS receiver. In fact, there is a constant bias between  $P_s$  and  $C/N_0$  in decibels under the assumption that  $N_0$  and  $B_n$  are constant during the observation period. In the following discussion, we do not discriminate between  $P_s$ , SNR, or  $C/N_0$ , and use  $P_s$  as the observable of the forward model.

Considering the reflected signal, the composite signal power is formulated as

$$P_s = P_d + P_r + 2\sqrt{P_d P_r} \cos \Phi_i \quad (2)$$

where  $P_d$  and  $P_r$  are the power of the direct and reflected signals, respectively, and  $\Phi_i$  is interference phase which amounts to the excess phase of the reflected wave with respect to the direct wave.

The change of  $\Phi_i$  determines the positions of the maxima and minima of the interference pattern of the observed signal power  $P_s$ , and the modulation amplitude (null depth) is determined by the factor  $2\sqrt{P_d P_r}$ . If we assume that the receiving antenna is working on a dominant polarization, then  $\Phi_i$  can be divided into three parts:

$$\Phi_i = \phi_g + \phi_r + \phi_a \quad (3)$$

where the term

$$\phi_g = \frac{4\pi h \sin e}{\lambda} \quad (4)$$

is the interference phase introduced by the geometrical path difference of the direct and reflected signals,  $h$  is the

geometrical antenna height above the reflecting surface,  $\lambda$  is the wave length of the electromagnetic (EM) wave (L1 is 1575.42 MHz and  $\lambda_{L1}$  is 19.0 cm) and  $e$  is the elevation angle of the GPS satellite. The term

$$\phi_r = \arg(R) \tag{5}$$

is the interference phase introduced by the reflection and amounts to the phase of the complex Fresnel reflection coefficient  $R$  which is polarization dependent. The term

$$\phi_a = \Theta(-e) - \Theta(e) \tag{6}$$

reflects the different phase response of the antenna at different elevation angles, where  $\Theta(e)$  is the phase pattern, i.e., the angle of the complex radiation pattern, of the receiving antenna at  $e$ .

Substituting  $x = \sin e$ ,  $f_M = 2h/\lambda$ , and (4) into (2), the signal power is

$$P_s = P_d + P_r + 2\sqrt{P_d P_r} \cos(2\pi f_M x + \phi_r + \phi_a) \tag{7}$$

We use Lomb-Scargle Periodogram (LSP) (Lomb 1976), which is similar to Fast Fourier Transform (FFT) but does not require evenly spaced sampling, to obtain the estimation of  $f_M$  (denoted as  $f_{eff}$ ), and then convert  $f_{eff}$  to reflector height by

$$h_{eff} = \frac{\lambda f_{eff}}{2} \tag{8}$$

The retrieved reflector height  $h_{eff}$  is not always equal to the geometrical reflector height  $h$  and has been referred to as the effective reflector height (Larson et al. 2010). It is demonstrated that  $h_{eff}$ , with a geodetic GPS antenna, can have a 0–5-cm offset to  $h$  for a bare soil case depending on the soil moisture level (Zavorotny et al. 2010). If the change of the interference phase is completely due to the movement of GPS satellite, i.e.,  $\Delta\Phi_i = \Delta\phi_g$ , then the retrieved effective reflector height is equal to the geometrical reflector height, i.e.,  $h_{eff} = h$ . If  $\phi_r$  is not constant but changing with elevation angle, then a reflector height bias  $\delta h = h_{eff} - h$  is brought in (Here we assume  $\phi_a = 0$ ) and can be calculated by

$$\delta h = \frac{\lambda}{4\pi} \frac{d\phi_r}{dx} \tag{9}$$

As will be illustrated later, the error term  $\delta h$  is non-negligible if the receiving antenna is vertically polarized.

The amplitude of the modulation term  $A_m = 2\sqrt{P_d P_r}$  can be further computed by (Nievinski and Larson 2014a)

$$A_m = 2|RS|\sqrt{G(e)G(-e)}P_{d,iso} \tag{10}$$

where  $P_{d,iso}$  is the received power of the direct GPS signal by an isotropic antenna (about  $-160$  dBW above earth surface),  $G(e)$  is the gain pattern, i.e., the magnitude of the

complex radiation pattern, of the receiving antenna at elevation angle  $e$ , and  $S$  is the attenuation factor introduced by the reflector roughness and can be computed by (Beckmann and Spizzichino 1987; Nievinski and Larson 2014a)

$$S = \exp(-0.5k^2 s^2 \cos^2 \theta) \tag{11}$$

where  $k = 2\pi/\lambda$  is the wave number in free space,  $\theta$  is the angle of incidence with respect to normal direction, and  $s$  is the standard deviation of the surface height.

Both the reflection coefficient  $R$  and the antenna gain  $G(e)$  are polarization dependent. Typically a geodetic GPS antenna works on RHCP, and the gain for an LHCP EM wave is at least 15 dB smaller for high elevation angles (Zavorotny et al. 2010). However, at low elevation angles the LHCP gain is comparable or even exceeds the RHCP gain. In fact, the discrepancy between  $h_{eff}$  and  $h$  is primarily due to the non-negligible LHCP gain of the geodetic GPS antenna at low elevation angles. Although  $P_d$  and  $P_r$  are affected by various factors, e.g.,  $R$ ,  $S$  and  $G(e)$ , the difficulty of retrieving  $f_{eff}$  (and thus  $h_{eff}$ ) is not obviously increased because their changes are much slower than those caused by the change of interference phase  $\Phi_i$  unless  $A_m$  is so small that the interference pattern vanishes.

The horizontal, vertical, RHCP to RHCP, and RHCP to LHCP reflection coefficients can be computed by (Balanis 2012)

$$R_h = \frac{\cos \theta_i - \sqrt{\epsilon_r - \sin^2 \theta_i}}{\cos \theta_i + \sqrt{\epsilon_r - \sin^2 \theta_i}} \tag{12}$$

$$R_v = \frac{\epsilon_r \cos \theta_i - \sqrt{\epsilon_r - \sin^2 \theta_i}}{\epsilon_r \cos \theta_i + \sqrt{\epsilon_r - \sin^2 \theta_i}} \tag{13}$$

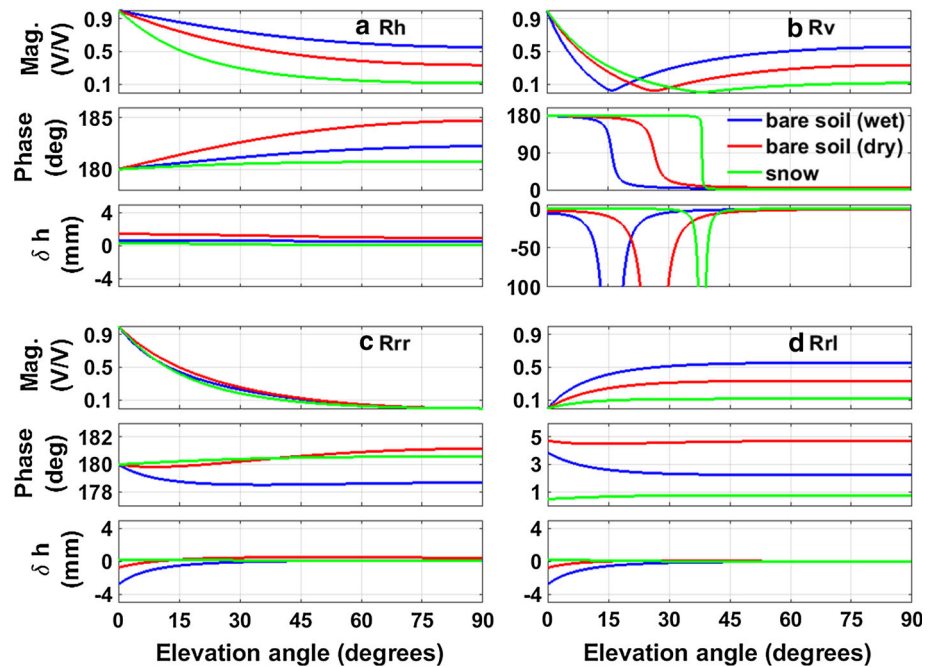
$$R_{rr} = \frac{1}{2}(R_v + R_h) \tag{14}$$

$$R_{rl} = \frac{1}{2}(R_v - R_h) \tag{15}$$

where  $\theta_i$  is the angle of incidence,  $\epsilon_r$  is the complex permittivity of the bottom medium, and the top medium is air ( $\epsilon_{r,air} = 1$ ).

The reflection coefficients for the four polarizations of wet soil ( $\epsilon_r = 12 + 1.5j$ ), dry soil ( $\epsilon_r = 4.5 + 0.5j$ ), and snow ( $\epsilon_r = 1.5 + 0.001j$ ) (Ulaby et al. 1981) together with reflector height bias  $\delta h$  are illustrated in Fig. 1. The reflection coefficients of the four polarizations show different characteristics which can be used in different remote sensing applications. The magnitude of  $R_v$  shows a notch at a particular elevation angle referred as the Brewster’s angle, which can be used to retrieve soil moisture and vegetation biophysical parameters (Rodriguez-Alvarez et al. 2009, 2011a, b). However, the sharp phase change

**Fig. 1** Fresnel reflection coefficients of **a** horizontal, **b** vertical, **c** RHC to RHC, **d** RHC to LHC polarizations. For each polarization, the reflection coefficients are calculated for three kinds of medium: wet soil, dry soil, and snow. For each plot, the *top* and *middle panels* are the magnitude and phase of the reflection coefficient. The *bottom panel* is the retrieved reflector height bias  $\delta h$  as a result of the change of the reflection coefficient phase



around the Brewster's angle would yield a significant retrieved reflector height error and thus makes vertical polarization unsuitable for geometry driven applications, such as snow depth and sea/water level monitoring. The horizontal polarization can be used to estimate snow depth for the large magnitude and the almost constant phase of the reflection coefficients. The latter guarantees that  $\Delta\Phi_i = \Delta\phi_g$  and thus the retrieved reflector height  $h_{\text{eff}}$  is equal to the geometrical reflector height  $h$ .

## Experimental setup and results

Previous discussion highlights that the polarization and gain pattern of the GPS antenna are the key factors to determine the performance of the GPS-IR technique. In this section, we first introduce an experimental setup in Marshall, Colorado, aimed at snow depth measurements. The snow depth measurements, together with the ground truth data and the air temperature, are then presented.

### Experimental setup

A snow monitor utilizing the dipole antenna proposed by Chen et al. (2014) has been installed at the experiment field of UCAR, Marshall, Colorado, USA (105°13.96'W, 39°56.98'N). The dipole antenna was horizontally oriented and directed south, and thus it is horizontally polarized with the east–west direction serving as the optimal sensing area. Because the horizontal polarization is utilized, we

designate this system the Horizontal Polarization Snow Monitor (HPSM).

Figure 2 shows the HPSM setup and optimal sensing area. A low-cost GlobalTop Gmm-u2P GPS evaluation board with a customized firmware to provide SNR resolved to 0.1 dB Hz served as the GPS L1 receiver. The customized dipole antenna and the receiver were placed inside a PVC housing which is water-proof and transparent to EM wave at L1 frequency. The PVC housing was mounted on top of an aluminum post which was approximately 2.7 m above the ground, as shown in the left panel of Fig. 2. A Panasonic Toughbook was used to record the SNR data. The antenna orientation and sensing area are illustrated in the middle panel of Fig. 2.

There is also a PBO geodetic station southeast of the HPSM, and they are about 25 m apart. This PBO GPS station includes a Trimble NetR9 receiver and a Trimble L1/L2 Dorne Margolin choke ring antenna which is about 2 m above the ground. The snow depth measurements from the PBO geodetic receiver are publicly available from <http://xenon.colorado.edu/portal/?station=p041>. The UCAR site also has ultrasonic SR50 snow sensors which are about 100 m south of the HPSM. In order to assist the evaluation of the snow depth measurements, we installed a camera and a labeled measurement post in the east direction (R01 and R16). An example image captured by the camera is given in the right panel of Fig. 2. The snow sensor system was functional from October 2013 and operated through May 2014. Occasional hardware failures resulted in some data loss during the test.



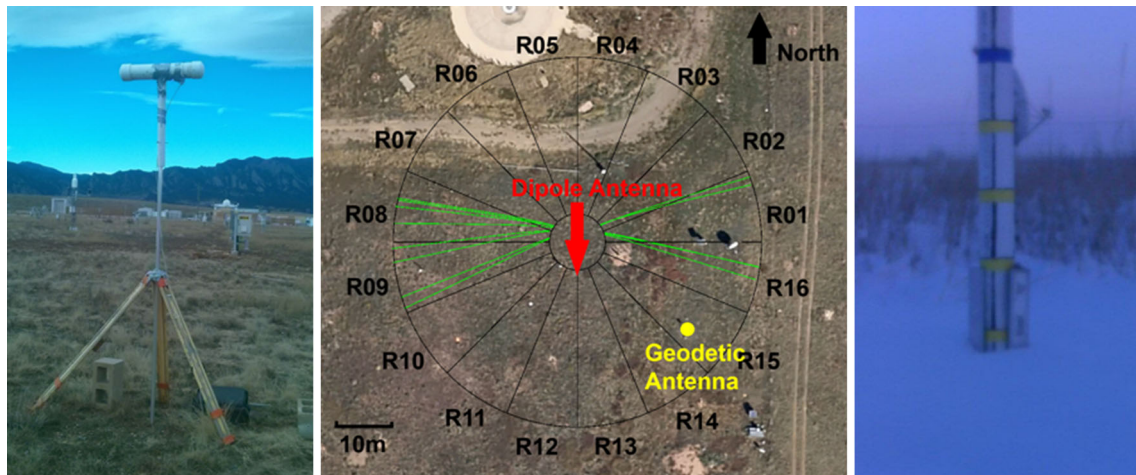


**Fig. 2** HPSM setup and sensing regions in Marshall Field, CO, USA. *Left* the dipole antenna and a low-cost GPS receiver are inside the white PVC housing. A laptop inside the *black box* is used to record GPS SNR data. *Middle* the dipole antenna is south oriented, so the east and west regions are the optimal sensing area. The whole region is divided into 16 sectors, and the 13 ground tracks located in sectors

R01, R16, R08, and R09 are used to retrieve snow depth. The radii of the outer and inner rings are 30.9 and 4.7 m, respectively, corresponding to elevation angles of 5° and 30°. *Right* image captured by the camera. The *blue label* on the post is 50 cm, and the interval between *yellow labels* is 10 cm

**Experimental results**

Before measuring snow depth, the antenna height with respect to bare soil needs to be computed using the LSP and serve as the calibration height. For each ground track, the antenna height measurements on several dry days are averaged to serve as the *j*-th calibration height  $H_j^{cal}$  ( $j = 1, 2, \dots, 13$ ). The standard deviations of used bare soil reflector heights range from 0.5 to 0.9 cm across the entire snow-free period. For the *i*-th day ( $i = 1, 2, 3, \dots$ ) and the *j*-th ground track ( $j = 1, 2, \dots, 13$ ), an antenna height  $H_{i,j}$  is obtained using LSP and the height difference  $sd_{i,j} = -H^{cal} - H_{i,j}$  is regarded as the measured snow depth for the *j*-th ground track on the *i*-th day. Then all the snow measurements within 1 day are averaged to get the *i*-th day’s snow depth:

$$sd_i = \frac{1}{M} \sum_{j=1}^M sd_{i,j} \tag{16}$$

where *M* is the number of usable ground tracks.

Some examples of the raw SNR and the corresponding LSPs before and after a snowfall are shown in Fig. 3. The raw SNR data of the three ground tracks in sector R16 on Day of Year (DoY) 306, 2013 and DoY 033, 2014 show clear interference patterns. There was no snow or any other precipitation on DoY 306, 2013 but approximately 13 cm snow on DoY 033, 2014. We can clearly see a frequency change between the 2 days’ SNR data. The interference pattern of the bare soil case is more distinct than that of the snow case, which indicates a stronger reflection power from bare soil than snow. This observation matches the

simulation result in Fig. 1. In Fig. 3d–f, the LSPs of the three ground tracks for the 2 days’ SNR are shown, indicating a reflector height change (i.e., snow depth) of approximately 13 cm.

The snow measurements from all four types of sensors together with the air temperature are shown in Fig. 4. In the top panel, the uncertainties of the HPSM measurements are based on the standard deviations of snow depth retrievals. The experiment period was from November 2, 2013 through May 20, 2014. In this period, there are eleven snowfall events, both heavy and light, and each snowfall is numbered and labeled with a narrow gray bar at the beginning. There is no heavy snowfall, and the maximum snow depth is about 15 cm (snowfall 2 and 5). Also there are some very light snowfalls which result in <5 cm snow depth (snowfall events 3, 4, 7, 8, 9, 10).

It is worth to note that we did not implement any error checking for HPSM snow depth measurements and non-sensical snow depths are retrieved occasionally. For example, for snowfall events 1, 3, and 4, HPSM tends to underestimate the true snow depth and even yields negative snow depth values. In contrast, for snowfall event 2 the HPSM tends to overestimate the actual snow depth as the SR50 and camera data indicate that the snow depth is decreasing, while the HPSM measurements give the opposite trend. Because of the small uncertainties, it is reasonable to assume that the measurement anomalies are systematic errors instead of measurement noise. For now, we put aside the measurement anomalies and will discuss that in next section.

**Fig. 3** Raw SNR data and corresponding Lomb-Scargle Periodograms of PRN 02, 14, 17 on DoY 306, 2013 and DoY 33, 2014. **a–c** SNR data of the three ground tracks in sector R16. They are all rising arcs, and the azimuth angles are 71.8°–95.8°, 72.3°–99.2°, and 73.3°–101.0°, respectively. **d–f** Corresponding Lomb-Scargle Periodograms computed for the SNR data

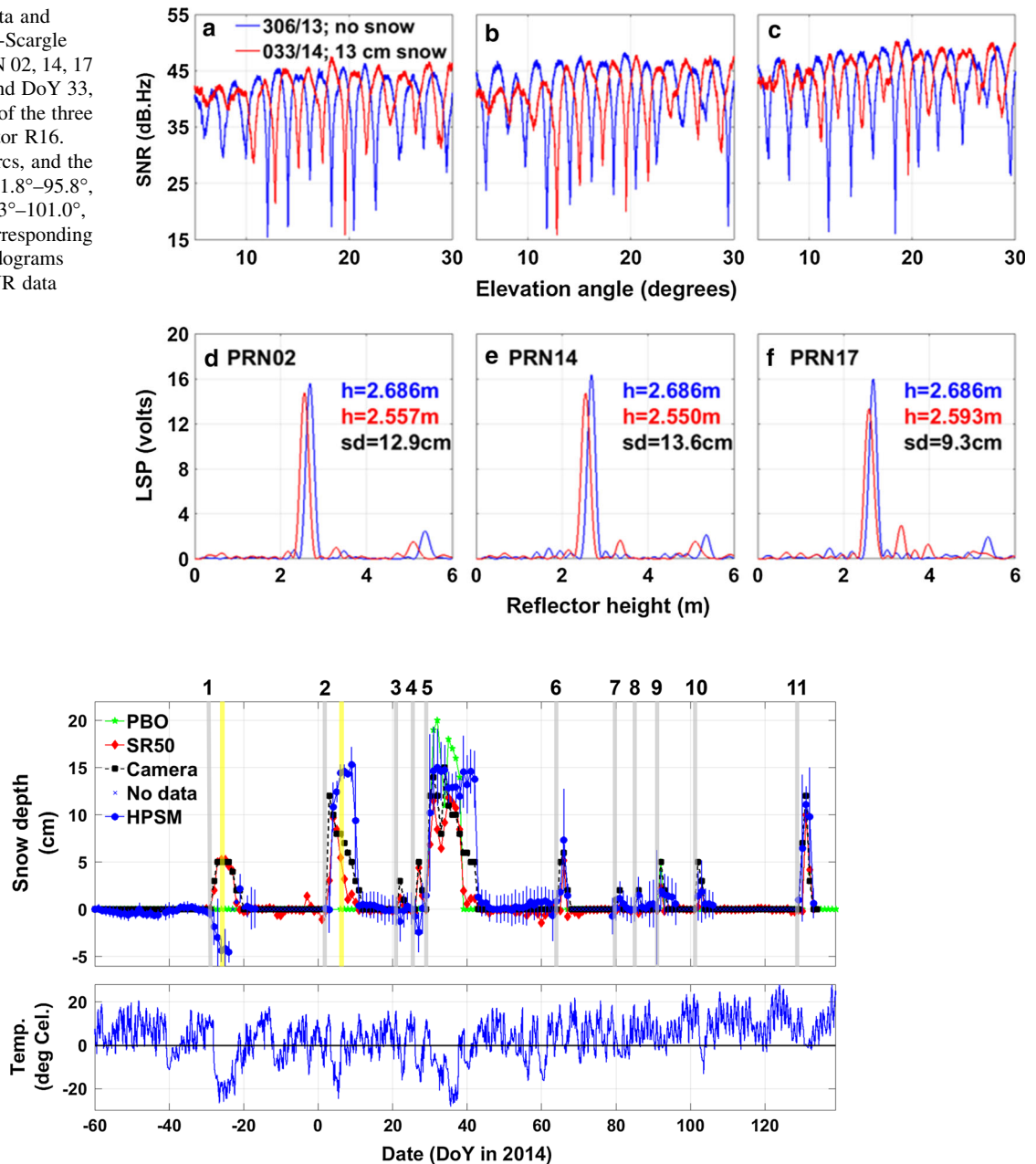


**Fig. 4** Snow depth measurements and air temperature data during the experiment period. The *top panel* is the snow depth measurements from the HPSM, the PBO geodetic GPS station, SR50 ultrasonic sensors, and the camera. There are 11 snowfalls from Nov 2013 to May 2014. The beginning of each snowfall is labeled by *gray bar*, and each snowfall is numbered. The snow conditions on the 2 days

labeled by the *yellow bars* will be discussed in the next section. The *error bars* are based on the standard deviation of the individual measurements. The *bottom panel* is the air temperature. The time unit is DoY in 2014, so the days in 2013 have a negative index (e.g., DoY 0, 2014 = DoY 365, 2013)

The measurements from the camera and the SR50 sensors match up well although they are not collocated. This indicates that the spatial variations of the snow depth at Marshall are small and thus the measurements from the camera and SR50 sensors can serve as the ground truth data. Regardless of the measurement anomalies, we can see that the HPSM is able to detect every snowfall event,

thereby indicating that the HPSM is very sensitive to even a small snow depth change. In contrast, the PBO geodetic snow sensor shows the least sensitivity by only detecting three of the snowfall events. Lacking the detailed specifics of the data processing algorithm, it is possible to speculate that the lack of snowfall detection may be a result of the lower reflection power and thus the deteriorated SNR fails

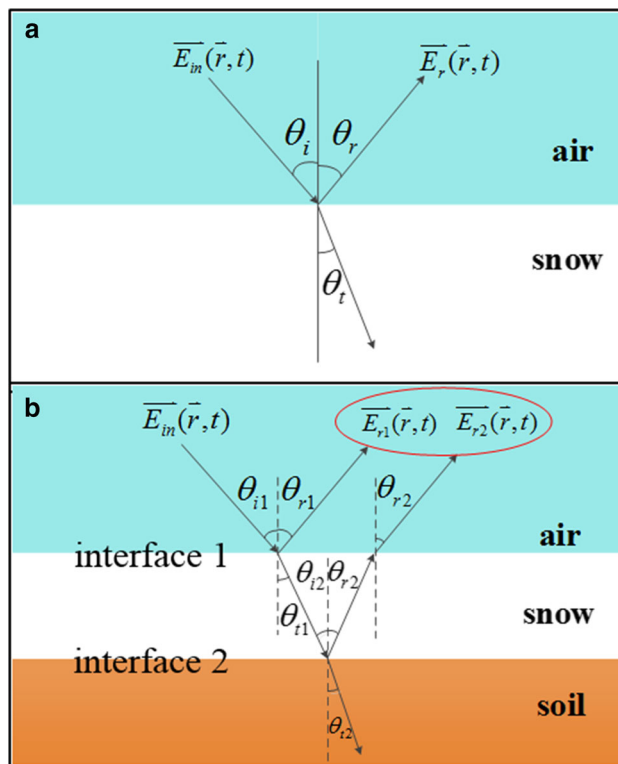
to pass the quality check mechanism and cannot yield a reasonable snow depth measurement.

### Model reconsideration

Although the HPSM measurement anomalies are small, these systematic errors need to be explained. In this section, a dual-interface model is proposed to account for the anomalies. This model is validated by comparing the simulation results with the HPSM measurements for two snowfall events with significant measurement anomalies. Finally a simulated estimation error curve is demonstrated using the dual-interface model given various snow conditions, i.e., snow depths and permittivities. The distribution of the HPSM measurements matches the simulated error curve.

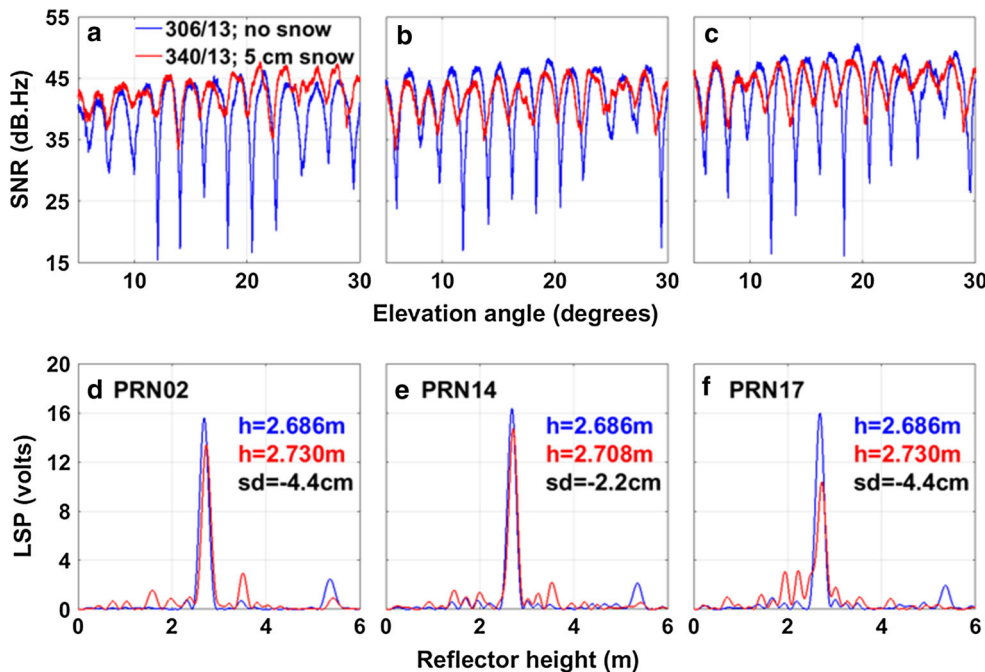
### Dual-interface model

In order to verify that the anomalies are not due to measurement noise, we show the SNR data and corresponding LSPs on DoY 340, 2013 (labeled by the left yellow bar in Fig. 4) of sector R16 in Fig. 5. On this day, the ground truth snow depth is about 5 cm, while the HPSM reports about  $-5$  cm snow measurements. In Fig. 5d–f, the corresponding LSPs show a negative snow depth from  $-2.2$  to  $-4.4$  cm. In addition, the measurements in other sectors



**Fig. 6** Two reflection models for snow depth retrievals. **a** Single-interface model. The incidence EM wave is bounced back on the air–snow interface. **b** Dual-interface model. Two leading reflections occur at the air–snow and snow–soil interfaces. In the air half space, the two reflected waves add up coherently

**Fig. 5** Raw SNR data and corresponding Lomb-Scargle Periodograms of PRN 02, 14, 17 on DoY 306 and 340, 2013. **a–c** SNR data of the three ground tracks in sector R16. They are all rising arcs, and the azimuth angles are  $71.8^\circ$ – $95.8^\circ$ ,  $72.3^\circ$ – $99.2^\circ$ , and  $73.3^\circ$ – $101.0^\circ$ , respectively. **d–f** Corresponding Lomb-Scargle Periodograms computed for the SNR data



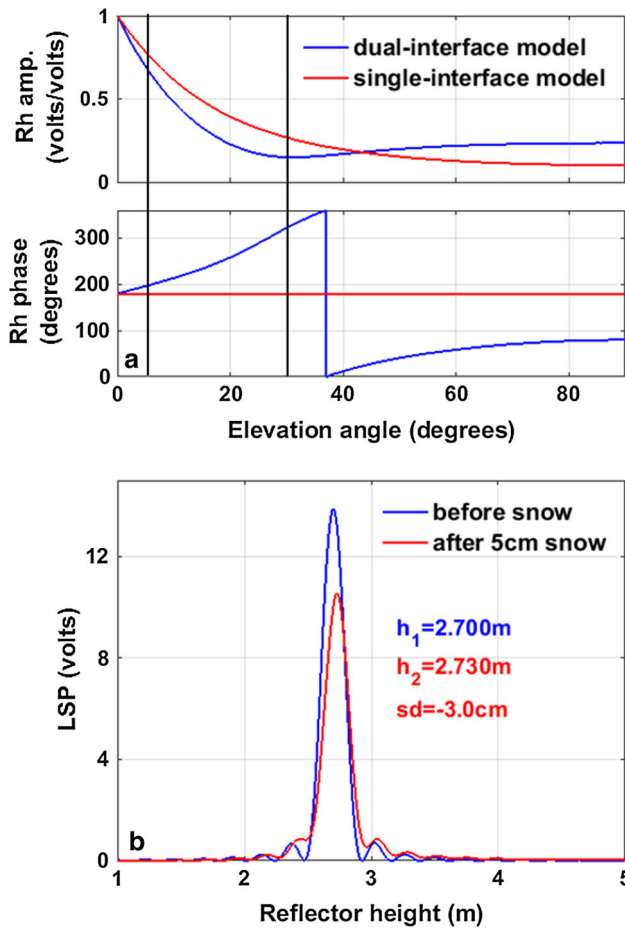


**Fig. 7** Reflection coefficients and Lomb-Scargle Periodograms using the dual-interface model with a 5-cm snow layer. **a** Horizontal reflection coefficients for the dual-interface model and the single-interface model. **b** LSPs corresponding to the bare soil and 5-cm snow are simulated using the dual-interface model. The simulated snow depth estimation is  $-3.2$  cm, while the actual snow depth is 5 cm. The elevation angle range used to calculate LSP is from  $5^\circ$  to  $30^\circ$  (between the dark bars)

also show negative snow depth from  $-2.9$  to  $-5.5$  cm which indicates that the anomalies cannot be explained by measurement noise, particularly given the clarity of the interference pattern.

In the previous simulation, reflection coefficients are computed under the single-interface model, i.e., the top medium (air) and bottom medium (soil or snow) occupy the entire half space (Fig. 6a). Under this model, there is only one reflection occurring on the air–snow (or air–soil) interface. However, in the actual environment, regardless of the depth of the snow layer, there is another soil layer beneath the snow layer (Fig. 6b). Although the influence of the underlying medium (soil) is frequently ignored in snow depth studies (Chew et al. 2015), it might be non-negligible for thin snow layer. If we account for the leading two outgoing reflections occurring at the air–snow and snow–

soil interfaces and neglect high-order bounces and the bottom interface roughness, then the two bounced-back EM waves,  $\vec{E}_{r1}(\vec{r}, t)$  and  $\vec{E}_{r2}(\vec{r}, t)$ , add up coherently and result in a composite reflection coefficient  $R_{\text{comp}}$  defined as

$$R_{\text{comp}} = \frac{\vec{E}_{r1}(\vec{r}, t) + \vec{E}_{r2}(\vec{r}, t)}{\vec{E}_{\text{in}}(\vec{r}, t)} \tag{17}$$

where  $\vec{E}_{\text{in}}(\vec{r}, t)$  is the incident EM wave. The composite horizontal reflection coefficients is computed by (Born and Wolf 1980)

$$R_{\text{comp}} = \frac{R^{(1)} + R^{(2)}Q}{1 + R^{(1)}R^{(2)}Q} \tag{18}$$

where the term

$$R^{(1)} = \frac{\cos \theta_i - \sqrt{\epsilon_{r1} - \sin^2 \theta_i}}{\cos \theta_i + \sqrt{\epsilon_{r1} - \sin^2 \theta_i}} \tag{19}$$

is the regular horizontal Fresnel reflection coefficient for the interface 1,  $\theta_i$  is the angle of incidence,  $\epsilon_{r1}$  is the permittivity of the middle medium (snow). The term

$$R^{(2)} = \frac{\sqrt{\epsilon_{r1} - \sin^2 \theta_i} - \sqrt{\epsilon_{r2} - \sin^2 \theta_i}}{\sqrt{\epsilon_{r1} - \sin^2 \theta_i} + \sqrt{\epsilon_{r2} - \sin^2 \theta_i}} \tag{20}$$

is the regular horizontal Fresnel reflection coefficient for the interface 2, and  $\epsilon_{r2}$  is the permittivity of the bottom medium (soil). The term add up coherently

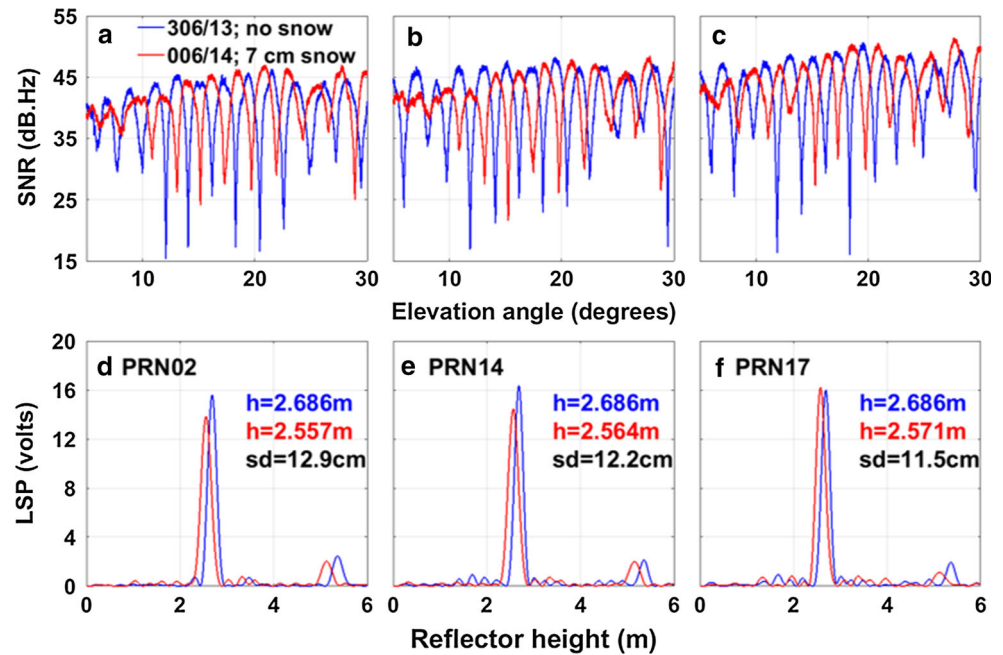
$$Q = \exp\left\{2jkH_{\text{snow}}\sqrt{\epsilon_{r1} - \sin^2 \theta_i}\right\} \tag{21}$$

accounts for a phase shift and amplitude attenuation due to the propagation within the snow layer.

Some studies also employ layered model in snow sensing applications. Rodriguez-Alvarez et al. (2012) propose to use a vertically polarized antenna to measure snow depth. Rather than estimating the frequency of the interference pattern, they utilize the number and positions of the multiple notches of the SNR, which arise from the layering effect, to retrieve the snow depth. However, there are more than one solution corresponding to the observed notches, and ancillary snow depth data are needed to resolve the uncertainty. Jacobson (2010) utilizes a horizon-looking geodetic Trimble antenna and a layered model, i.e., snow + lake ice, to retrieve lake ice thickness using a least square method. However, the least square method requires a priori knowledge of the environment, such as snow thickness on top of lake ice, and it could converge to difference solutions depending on the accuracy of the a priori knowledge. Cardellach et al. (2012) employ the cross-correlation waveform, rather than the SNR, from a horizon-looking geodetic antenna as the observable. Then a spectral



**Fig. 8** Raw SNR data and corresponding Lomb-Scargle Periodograms of PRN 02, 14, 17 on DoY 306, 2013 and DoY 6, 2014. **a–c** SNR data of the three ground tracks in sector R16. **d–f** Corresponding Lomb-Scargle Periodograms computed for the SNR data



analysis is performed, for different time lags with respect to the direct signal, to detect the sub-structure of dry snow in Antarctica area. The technique utilizes the code modulation of the GPS C/A signal on L1 frequency, and it is applicable to detect layers far apart but is not suitable for closely separated layers.

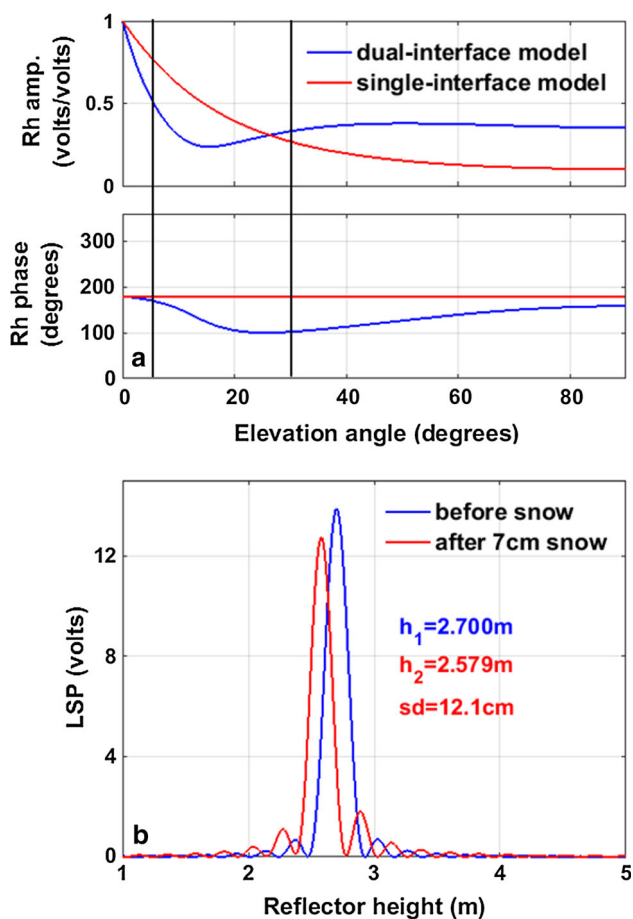
Utilizing (17–21), we can simulate the composite reflection coefficient for horizontal polarization and then compute the LSP from the simulated data. Because measurement anomalies are not expected, we did not make a field survey to measure the permittivities of snow and soil. However, we can use previous experiments carried out at the same location (Marshall Field, UCAR) to obtain an approximation. Zavorotny et al. (2010) use in situ volumetric water content (VWC) to infer a relatively stable surface soil permittivity of  $4.5 + 0.5j$  at Marshall, provided the VWC is not changed significantly by precipitation. When the temperature is below  $0^\circ\text{C}$ , the complex permittivity of soil, both real and imaginary components, can have a reduction as the temperature decreases due to the freezing of water (Hallikainen et al. 1985; Mironov et al. 2010). For the relatively dry soil in Marshall, the impact of temperature change is not as significant as densely wet soil. For the dual-interface model to be used in this study, a soil permittivity value from  $4.0 + 0j$  to  $4.5 + 0.5j$  is a reasonable approximation. For new snow in the experiment location, a permittivity value from 1.4 to 1.8 is a reasonable approximation—the imaginary part of snow permittivity is usually small enough to be neglected. In the simulation, the permittivities of the snow and soil medium are set to be  $1.5 + 0.001j$  and  $4.3 + 0.3j$ , respectively.

Figure 7 shows the horizontal reflection coefficients with a 5-cm snow layer under both single-interface and dual-interface models and the corresponding LSPs. In Fig. 7a, we can see that the amplitude is smaller than that of the single-interface model, which would cause the fringes of the SNR interference pattern to be less distinct. More notably, the phase is no longer consistent but increases as the elevation angle increases. This changing phase would introduce a reflector height bias  $\delta h$  as illustrated by (9). The LSP using the dual-interface model assuming a 5-cm snow layer is given in Fig. 7b. The antenna height above the bare soil ground is 2.7 m, and its LSP shows a strong frequency component at  $h = 2.7$  m. Adding a 5-cm snow layer, the LSP shows a frequency component at  $h = 2.73$  m, resulting in a  $-3.0$  cm snow depth, while the actual geometric antenna height is 2.65 m. The simulated LSPs match those of the ground tracks in R16 as shown in Fig. 5.

### Model verification and error curve

Another anomaly in the HPSM snow measurements is the second snowfall event. The HPSM obviously overestimates the snow depth compared to the ground truth data. Again we will look at the LSPs of the actual data and see whether they match the simulation results. In Fig. 8, SNR data and LSPs of the three ground tracks in R16 on DoY 6, 2014 (labeled by the right yellow bar in Fig. 4) are shown. The HPSM snow depth measurement is about 12.5 cm, and the ground truth is about 7 cm.

In the simulation, the antenna height with respect to bare soil surface is 2.7 m and then a 7-cm snow layer is added.



**Fig. 9** Reflection coefficients and Lomb-Scargle Periodograms using the dual-interface model for a 7-cm snow layer. **a** Horizontal reflection coefficients for the dual-interface model and the single-interface model for a 7-cm snow layer. **b** LSPs corresponding to the bare soil and 7-cm snow are simulated using the dual-interface model. The simulated snow depth estimation is 12.1 cm, while the actual snow depth is 7 cm. The elevation angle range used to calculate LSP is from 5° to 30° (between the *dark bars*)

The same permittivities of snow and soil are used as those in the previous simulation. The simulated composite reflection coefficients and the LSPs are shown in Fig. 9. Instead of increasing with elevation angle, the composite reflection phase shows a decreasing trend with the elevation angle in the selected elevation angle range (5°–30°). This decreasing trend would introduce a negative bias to the antenna height estimation and thus make the snow depth overestimated. From Fig. 9b, we can see that the simulated LSPs match those of the observed data in Fig. 8 and the estimated snow depths are close.

It is clearly seen that the soil layer can cause a bias, either positive or negative, to the reflector height estimation. The estimation error is related with the depth of the snow layer as well as its permittivity. In order to understand the effect of the snow layer's depth and permittivity to the estimation errors, we simulate the estimation errors

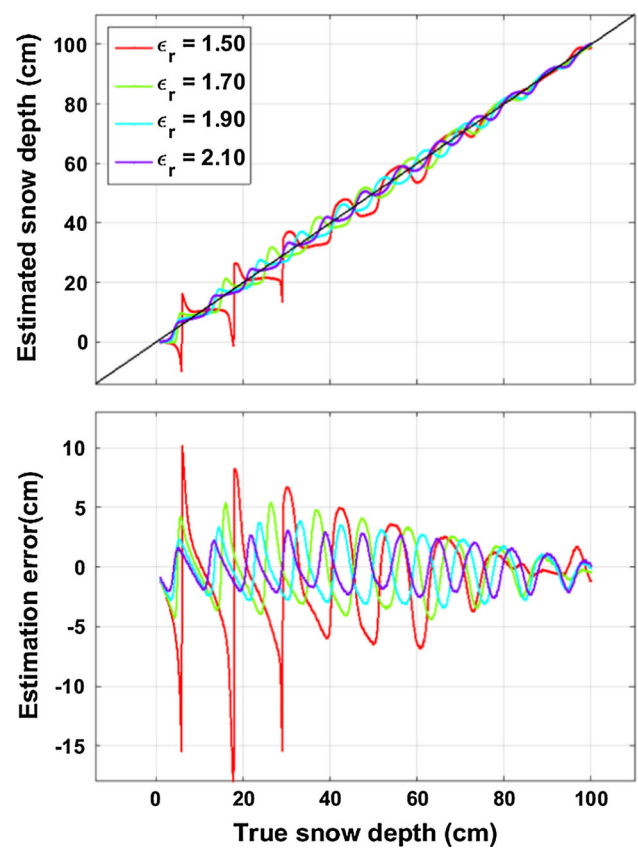


**Fig. 10** Snow depth estimation and estimation errors for various snow conditions, i.e., snow depth and permittivity. The *top panel* is the estimated snow depth versus true snow depth for various snow permittivity values. The elevation angle range used for reflector height retrieval is from 5° to 30°. The *bottom panel* is estimation error versus true snow depth

over a range of snow depth and the permittivity values. The error curve is shown in Fig. 10. We can see that the estimated snow depth varies around the true snow depth and the error is decreasing with the increment of snow depth. Also the estimation error decreases with increasing permittivity of snow layer. This is reasonable because a higher snow permittivity would allocate more energy to the first interface reflection and less to the bottom interface reflection. So the bottom interface reflected EM wave would have less influence on the top interface bounced EM wave, which is closer to the single-interface model.

With the simulated error curve, we can see whether the HPSM snow depth measurements match the simulated distribution. In Fig. 11, we superimpose the scatterplot of snow measurements on the error curve of  $\epsilon_r = 1.5$ . The *x* axis of the scatterplot is the ground truth data, and the *y* axis is the HPSM snow depth measurements. The elevation angle cutoff range is from 5° to 30°. We can see that the distribution of the HPSM snow depth measurements follows the simulated error curve to a reasonable extent. From Figs. 7 and 9, we can see that the changing rate of the

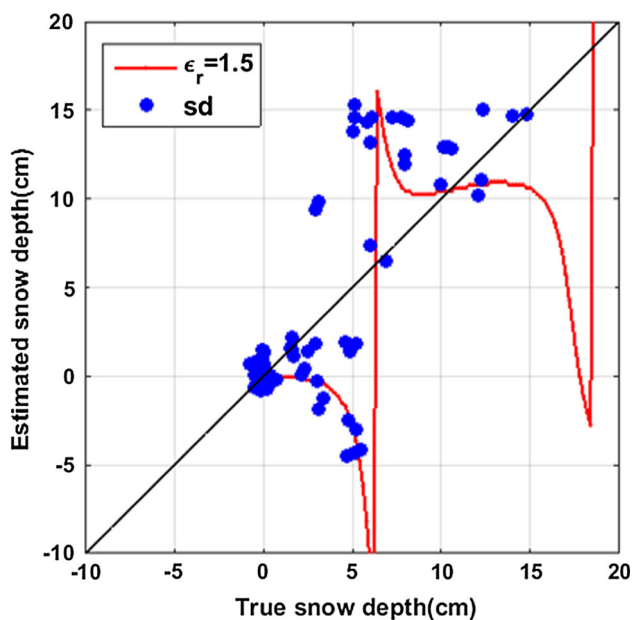


**Fig. 11** Simulated and observed snow depth measurements distribution. The *blue dots* are the scatter plots of retrieved snow depth versus ground truth. The *red curve* is the estimated snow depth corresponding to  $\epsilon_r = 1.5$ . The elevation angle range is from  $5^\circ$  to  $30^\circ$

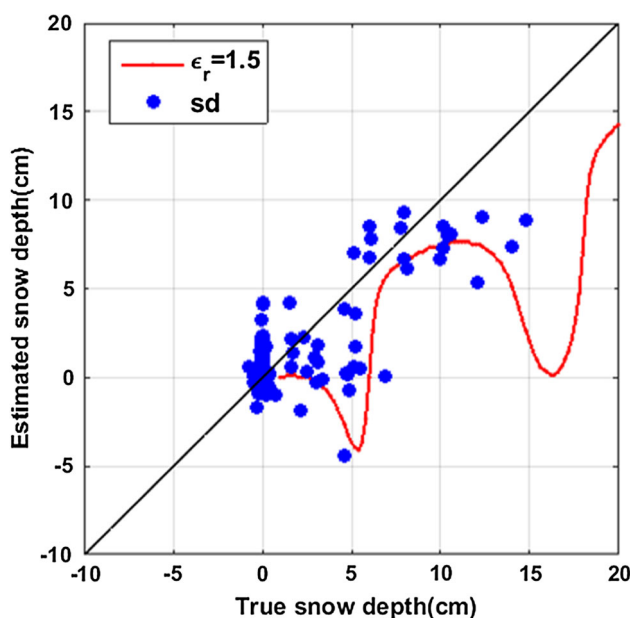


**Fig. 12** Simulated and observed snow depth measurements distribution. The *blue dots* are the scatter plots of retrieved snow depth versus ground truth. The *red curve* is the estimated snow depth corresponding to  $\epsilon_r = 1.5$ . The elevation angle range is from  $15^\circ$  to  $50^\circ$

reflection coefficient phase is not constant across the entire elevation angle range, indicating that the snow depth retrievals could be different if other elevation angle cutoffs are used. In order to further validate the dual-interface model, we re-calculate the snow depth measurements from

the SNR data using a higher elevation angle range from  $15^\circ$  to  $50^\circ$ . The scatterplot together with the simulated error curve is shown in Fig. 12, which also indicates good agreement between the HPSM measurements and simulation results.

This dual-interface model can explain the observed measurement anomalies; however, it illustrates the difficulty of isolating the reflector height bias because of the layering effect from the effective reflector height. In order to better discriminate the reflections from layers interfaces, different polarizations may be effective to obtain a better understanding of the environmental parameters.

## Conclusions

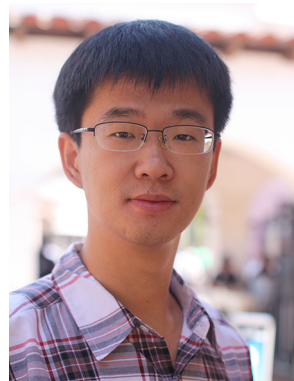
This study documents an experiment conducted at Marshall, CO, USA, during the 2013–2014 water year aimed to comprehensively assess the performance a dipole antenna for snow depth sensing. The developed instrument, designated HPSM, shows higher sensitivity to light snowfalls which should be attributed to the horizontal polarization and improved gain pattern of the antenna developed. In order to explain the observed measurement anomalies visible with the higher sensitivity, we propose a dual-interface model that accounts for the effect of the underlying medium and simulate the horizontal reflection coefficients. The phase of the horizontal reflection coefficients is changing as elevation angle increases, which brings in an estimation bias of the reflector height. In order to validate the proposed model, we simulate the LSPs for two snowfall events that encounter obvious measurement anomalies and the simulation results match the observed LSPs. With the dual-interface model, we simulate the estimation error curve for various snow depths and permittivities and find that the estimation error would decrease if the snow layer thickness and permittivity increase. The scatterplots of the HPSM measurements versus ground truth data, for two different elevation angle ranges, match well with the simulated distribution and thereby further validate the dual-interface model.

**Acknowledgments** The authors would thank Dr. John Braun of UCAR and Dr. Staffan Backén for their help in installing the instrument at Marshall Field. The authors would also thank Dr. Valery Zavorotny of NOAA for his invaluable help in the mathematical modeling.

## References

- Armstrong RL, Brun E (2008) Snow and climate: physical processes, surface energy exchange and modeling. Cambridge University Press, Cambridge

- Balanis CA (2012) *Advanced engineering electromagnetics*. Wiley, New York
- Barnett TP, Adam JC, Lettenmaier DP (2005) Potential impacts of a warming climate on water availability in snow-dominated regions. *Nature* 438:303–309. doi:[10.1038/nature04141](https://doi.org/10.1038/nature04141)
- Beckmann P, Spizzichino A (1987) *The scattering of electromagnetic waves from rough surfaces*. Artech House Inc., Norwood, MA
- Born M, Wolf E (1980) *Principles of optics*. Pergamon Press, Oxford
- Cardellach E, Fabra F, Rius A, Pettinato S, D'Addio S (2012) Characterization of dry-snow sub-structure using GNSS reflected signals. *Remote Sens Environ* 124:122–134. doi:[10.1016/j.rse.2012.05.012](https://doi.org/10.1016/j.rse.2012.05.012)
- Chen Q, Won D, Akos DM (2014) Snow depth sensing using the GPS L2C signal with a dipole antenna. *Eurasip J Adv Sig Process*. doi:[10.1186/1687-6180-2014-106](https://doi.org/10.1186/1687-6180-2014-106)
- Chew CC, Small EE, Larson KM, Zavorotny VU (2015) Vegetation sensing using GPS-interferometric reflectometry: theoretical effects of canopy parameters on signal-to-noise ratio data. *IEEE Trans Geosci Remote Sens* 53(5):2755–2764. doi:[10.1109/Tgrs.2014.2364513](https://doi.org/10.1109/Tgrs.2014.2364513)
- Gutmann ED, Larson KM, Williams MW, Nievinski FG, Zavorotny V (2012) Snow measurement by GPS interferometric reflectometry: an evaluation at Niwot Ridge, Colorado. *Hydrol Process* 26(19):2951–2961. doi:[10.1002/hyp.8329](https://doi.org/10.1002/hyp.8329)
- Hallikainen MT, Ulaby FT, Dobson MC, Elrayes MA, Wu LK (1985) Microwave dielectric behavior of wet soil. 1. Empirical-models and experimental-observations. *IEEE Trans Geosci Remote Sens* 23:25–34. doi:[10.1109/Tgrs.1985.289497](https://doi.org/10.1109/Tgrs.1985.289497)
- Jacobson MD (2010) Snow-covered lake ice in GPS multipath reception: theory and measurement. *Adv Space Res* 46(2):221–227. doi:[10.1016/j.asr.2009.10.013](https://doi.org/10.1016/j.asr.2009.10.013)
- Larson KM, Gutmann ED, Zavorotny VU, Braun JJ, Williams MW, Nievinski FG (2009) Can we measure snow depth with GPS receivers. *Geophys Res Lett* 36:L17502. doi:[10.1029/2009gl039430](https://doi.org/10.1029/2009gl039430)
- Larson KM, Braun JJ, Small EE, Zavorotny VU, Gutmann ED, Bilich AL (2010) GPS multipath and its relation to near-surface soil moisture content. *IEEE J Sel Top Appl Earth Observ* 3(1):91–99. doi:[10.1109/Jstars.2009.2033612](https://doi.org/10.1109/Jstars.2009.2033612)
- Lomb NR (1976) Least-squares frequency-analysis of unequally spaced data. *Astrophys Space Sci* 39(2):447–462. doi:[10.1007/Bf00648343](https://doi.org/10.1007/Bf00648343)
- Mironov VL, De Roo RD, Savin IV (2010) Temperature-dependable microwave dielectric model for an arctic soil. *IEEE Trans Geosci Remote Sens* 48(6):2544–2556. doi:[10.1109/Tgrs.2010.2040034](https://doi.org/10.1109/Tgrs.2010.2040034)
- Nievinski FG, Larson KM (2014a) Forward modeling of GPS multipath for near-surface reflectometry and positioning applications. *GPS Solut* 18(2):309–322. doi:[10.1007/s10291-013-0331-y](https://doi.org/10.1007/s10291-013-0331-y)
- Nievinski FG, Larson KM (2014b) Inverse modeling of GPS multipath for snow depth estimation-part I: formulation and simulations. *IEEE Trans Geosci Remote Sens* 52(10):6555–6563. doi:[10.1109/Tgrs.2013.2297681](https://doi.org/10.1109/Tgrs.2013.2297681)
- Nievinski FG, Larson KM (2014c) Inverse modeling of GPS multipath for snow depth estimation-part II: application and validation. *IEEE Trans Geosci Remote Sens* 52(10):6564–6573. doi:[10.1109/Tgrs.2013.2297688](https://doi.org/10.1109/Tgrs.2013.2297688)
- Rodriguez-Alvarez N, Bosch-Lluis X, Camps A, Vall-Ilossera M, Valencia E, Marchan-Hernandez JF, Ramos-Perez I (2009) Soil moisture retrieval using GNSS-R techniques: experimental results over a bare soil field. *IEEE Trans Geosci Remote Sens* 47(11):3616–3624. doi:[10.1109/Tgrs.2009.2030672](https://doi.org/10.1109/Tgrs.2009.2030672)
- Rodriguez-Alvarez N et al (2011a) Review of crop growth and soil moisture monitoring from a ground-based instrument implementing the interference pattern GNSS-R technique. *Radio Sci* 46(6):3. doi:[10.1029/2011rs004680](https://doi.org/10.1029/2011rs004680)
- Rodriguez-Alvarez N et al (2011b) Land geophysical parameters retrieval using the interference pattern GNSS-R technique. *IEEE Trans Geosci Remote Sens* 49(1):71–84. doi:[10.1109/TGRS.2010.2049023](https://doi.org/10.1109/TGRS.2010.2049023)
- Rodriguez-Alvarez N et al (2012) Snow thickness monitoring using GNSS measurements. *IEEE Trans Geosci Remote Sens Lett* 9(6):1109–1113. doi:[10.1109/Lgrs.2012.2190379](https://doi.org/10.1109/Lgrs.2012.2190379)
- Shi JC, Dozier J (2000) Estimation of snow water equivalence using SIR-C/X-SAR, part I: inferring snow density and subsurface properties. *IEEE Trans Geosci Remote Sens* 38(6):2465–2474. doi:[10.1109/36.885195](https://doi.org/10.1109/36.885195)
- Ulaby FT, Moore RK, Fung AK (1981) *Microwave remote sensing: active and passive*, vol 3. Addison-Wesley, Reading, MA
- Zavorotny VU, Larson KM, Braun JJ, Small EE, Gutmann ED, Bilich AL (2010) A physical model for GPS multipath caused by land reflections: toward bare soil moisture retrievals. *IEEE J Sel Top Appl Earth Observ* 3(1):100–110. doi:[10.1109/Jstars.2009.2033608](https://doi.org/10.1109/Jstars.2009.2033608)



**Qiang Chen** received his B.S. and M.S. degrees in electronic engineering from Tsinghua University, Beijing, China, in 2008 and 2011, respectively. He is currently working toward the Ph.D. degree in Astrodynamics and Satellite Navigation Systems in the Department of Aerospace Engineering Sciences, University of Colorado, Boulder, CO, USA. His research focuses on instrument design for GPS Interferometric Reflectometry remote sensing.



**Daehee Won** is a Research Associate at the Department of Aerospace Engineering Sciences, University of Colorado, Boulder, CO, USA. His research interests include multiple sensor integration (GPS, INS, vision), GNSS precise positioning (PPP, DGPS, RTK), navigation fault detection, nonlinear estimation (EKF, UKF, PF), GPS-IR remote sensing, and other navigation applications.





**Dennis M. Akos** received his Ph.D. degree in electrical engineering from Ohio University in the Avionics Engineering Center, Athens, OH, USA, in 1997. He is currently a professor in the Department of Aerospace Engineering Sciences, University of Colorado, Boulder, CO, USA. His research interests include GNSS, software-defined radio, digital signal processing, and radio-frequency design.